Analysis of the Forbush Decreases and Ground-Level Enhancement on September 2017 Using Neutron Spectrometers Operated in Antarctic and Midlatitude Stations

Guillaume Hubert, Maurizio T. Pazianotto, Claudio Antonio Federico, P. Ricaud

Analysis of the Forbush Decreases and Ground-Level Enhancement on September 2017 Using Neutron Spectrometers Operated in Antarctic and Midlatitude Stations

G. Hubert[1] [iD], **M. T. Pazianotto[2], C. A. Federico[3]** [iD], **and P. Ricaud[4]** [iD]

[1]ONERA/DPHY, University of Toulouse, France, [2]Instituto Tecnológico de Aeronáutica, São José dos Campos, Brazil, [3]Instituto de Estudos Avançados, São José dos Campos, Brazil, [4]Météo-France, Toulouse, France

Abstract This work investigates solar events occurred in September 2017 characterized by a series of Forbush decreases and a ground level enhancement (GLE). Forbush decreases is a rapid decrease in the observed https://en.wikipedia.org/wiki/Galactic_cosmic_ray intensity following a coronal mass ejection while GLE is induced by a strong solar event for which the flux of high-energy solar particles is sufficient to enhance the radiation level on the ground. These investigations were performed using data recorded by a neutron spectrometer network composed of a Bonner sphere system. Two instruments located at Pic-du-Midi Observatory (+2,885 m above sea level) and at Concordia station (Antarctica, +3,233 m) record simultaneously and continuously the neutron spectra, allowing to consider short-term variations during solar events. The main objective is to analyze neutron spectral properties including their energy distributions and dynamics. This paper presents cosmic ray-induced neutron spectra during active solar event leading to changes in the local cosmic ray spectrum (Forbush decreases and a GLE). Concerning the GLE, analyses show that neutrons in the evaporation domain are particularly amplified during the GLE, while other energetic domains increase uniformly.

1. Introduction

The characterization of radiations in the atmosphere is essential since secondary particles produced by primary cosmic rays (CR) are ubiquitous. The knowledge of the atmospheric radiation and physical mechanisms influencing its dynamic is an essential issue in some fields. Indeed, the atmospheric radiation knowledge is required to quantify effects on electronics system (Hubert et al., 2013; Hubert, Artola, et al., 2015; Hubert, Li Cavoli, et al., 2015; Lambert et al., 2005; Lambert et al., 2006; Peronnard et al., 2009), to assess the radiation risks for aircrews (Goldhagen et al., 2004; Hubert & Aubry, 2017a; Hubert & Aubry, 2017b; Reitz, 1993) but also in the framework of applications such as the muon tomography (Morishima et al., 2017) or the cosmogenic nuclide dating (Dunai, 2015). Indeed, cosmogenic nuclide dating uses the interactions between CRs and nuclides in glacially transported boulders or glacially eroded bedrock to provide age estimates for rock at the Earth's surface.

The primary CRs, mainly composed of protons and alphas, interact with atmospheric atoms, producing secondary particles such as neutrons, protons, muons, pions, or electrons (Grieder, 2001). Neutrons are the most studied particles due to their high fluxes, induced effects, and the ability to discriminate them. At ground level, other mechanisms contribute to neutron fluxes and their dynamics: the interaction between alpha particles emitted by radon and nuclei of elements from the atmosphere and crust (Kuzhevskij et al., 2001), the weather condition (Eroshenko et al., 2008; Lockwood & Yingst, 1956; Mishev & Stamenov, 2009), or seismic activities (Kuzhevskij et al., 2001). Moreover, atmospheric neutrons can be possibly generated by internal atmospheric mechanisms as lightning discharges (Libby & Lukens, 1973; Martin & Alves, 2010).

During quiet solar periods, the galactic cosmic ray spectrum is often described using the Force Field model (Gleeson & Axford, 1968) which considers the solar modulation potential as a time-dependent parameter. When directed toward Earth, the coronal mass ejections (CMEs) provoke Forbush decreases (FDs) (Forbush, 1937). The FD properties depend on several parameters such as the solar wind velocity
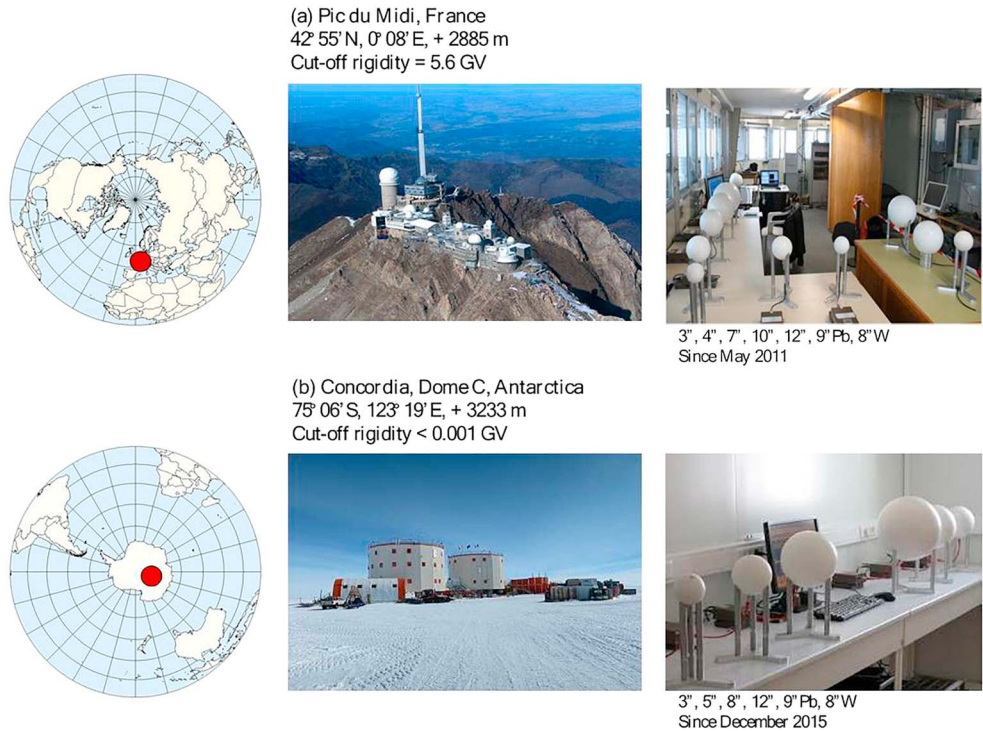
(a) Pic du Midi, France
42° 55' N, 0° 08' E, + 2885 m
Cut-off rigidity = 5.6 GV

3", 4", 7", 10", 12", 9" Pb, 8" W
Since May 2011

(b) Concordia, Dome C, Antarctica
75° 06' S, 123° 19' E, + 3233 m
Cut-off rigidity < 0.001 GV

3", 5", 8", 12", 9" Pb, 8" W
Since December 2015

Figure 1. Characteristics of the neutron spectrometers operated at the Concordia station and the Pic du Midi observatory.
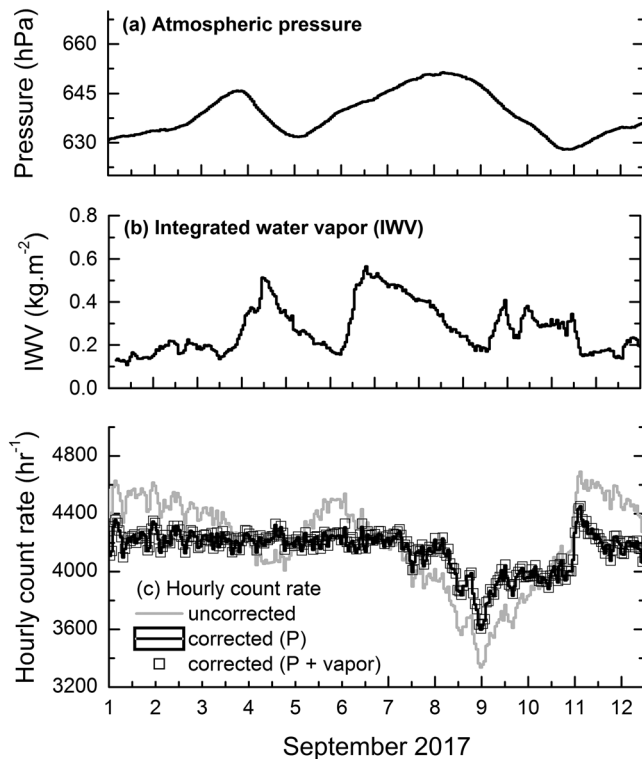

Figure 2. (a) Atmospheric pressure, (b) integrated water vapor IWV from the surface to the tropopause, and (c) uncorrected and corrected (pressure and pressure + water vapor) hourly count rate obtained for the 9″ lead sphere (from 1 to 13 September 2017).

or the interplanetary magnetic field when the disturbance crosses the Earth orbit (Cane, 2000). Moreover, additional particles may be induced in the atmosphere by solar energetic particles (SEP), with relatively short periods in the order of a few hours to a few days. Physical properties of these solar CR depend on some mechanisms including their source site, acceleration processes, coronal transport, and transport of accelerated particles through the interplanetary magnetic field (Ryan & Lee, 1991). In addition, the geomagnetic field affects the CR transport in its influence area, inducing charged particle flux redistribution. During these processes, the geomagnetic cutoff rigidities may become lower, allowing the entrance of additional particles into the atmosphere. This can be estimated using models (Dorman et al., 1972; McCracken et al., 1962; Shea et al., 1965) and methods describing the charged particle trajectories in the magnetic field of the magnetosphere.

Typical SEP events involve solar particles with energies lower than 0.1 GeV/n. These low-energy SEPs are totally absorbed in the upper atmosphere and do not reach ground. Nevertheless, during strong solar events that occur several times per decade, solar particle energies and fluxes may be sufficient to increase radiation levels on ground. Indeed, solar particle energies can reach up to 1–10 GeV/n during these events called ground level enhancements (GLE), and they can reinforce the atmospheric air shower cascade of secondary particles.

Neutron monitors (NMs) are used since the 1950s to record the atmospheric neutrons and protons. About 50 instruments distributed in different regions are currently networked, and particularly in the low cutoff rigidity regions (Hatton & Carmichae, 1964; Moral et al., 1993; WDC-
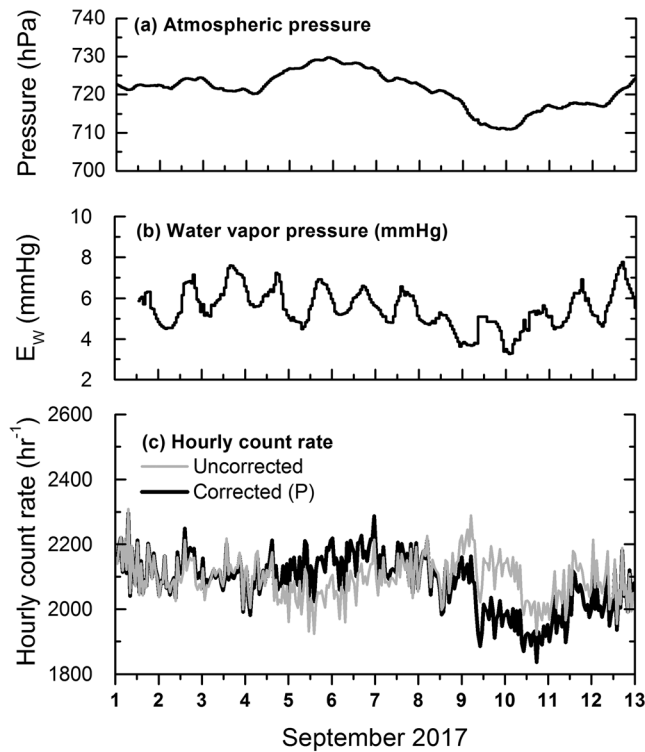
Figure 3. (a) Atmospheric pressure, (b) water vapor pressure, and (c) uncorrected/corrected (pressure) hourly count rate obtained for the 9″ lead sphere measured in the Pic du Midi during the period from 1 to 13 September 2017.

CR, http://cidas.isee.nagoya-u.ac.jp/WDCCR/). Thus, analyses and models on FD and GLE are derived from these measurements. More recently, the extended range Bonner Sphere Spectrometer (Cheminet et al., 2012; Hubert et al., 2004; Kim & Park, 2012; Pioch et al., 2011) were operated to investigate neutron spectra which enrich information by accessing the neutron energy distributions and their dynamic. A neutron spectrometer network was operated since 2015, with two main platforms located in the Pic-du-Midi observatory (France) and in the Concordia station (South Pole), respectively (Hubert, Li Cavoli, et al., 2015; Hubert, 2016). During the operational phase of measurements, especially in September 2017, neutron fluxes and spectra were monitored. In September 2017, the Sun was very active and presented a significant number of flares during the first half of the month. After a series of major flares including 27 M-class and 4 X-class flares, the solar active region that had produced an X9.3 flare on 6 September induced some FDs. Solar activity decreased on 9 and 10 September but on 10 September, a X8.2 class solar flare induced solar energetic particles with high energies. This flare led to the second GLE of the current solar cycle, identified as GLE #72 (GLE database, http://gle.oulu.fi/). For the first time, a solar flare involving a series of FDs and a GLE has been recorded simultaneously by several neutron spectrometers.

This paper presents analyses of the CR-induced neutron spectra during a solar event implying FDs and GLE. Neutron spectra recorded at Pic-du-Midi observatory and Concordia station were analyzed and compared with NMs data issued from Antarctica region.

2. High-Altitude Stations and Platform Descriptions

2.1. Concordia and Pic du Midi Station/Observatory

A neutron spectrometer was developed to record and study the neutron spectrum considering energy range from thermal region up to GeV (Cheminet et al., 2012). As described in previous works (Cheminet et al., 2012; Hubert, Federico, et al., 2016), the instrument is based on multisphere spherical [3]He proportional counters, placed in spherical moderators with different diameters and consisting of high-density polyethylene. To reach the response to neutrons above 20 MeV, the spectrometer includes two spheres with lead and tungsten shells.

Three neutron spectrometers are currently operated simultaneously. The first two instruments are operated in the Pic-du-Midi Observatory and in the Pico dos Dias Observatory since May 2011 and 2015, respectively (Hubert, Federico, et al., 2016). The Chinstrap project, supported by the French Polar Institute (IPEV), aims at recording neutron spectra at the Concordia station (+3,233 m) located near the top of the dome C. Thus, the third instrument was installed in December 2015 (Hubert, 2016; Hubert, 2017b), and it constantly measures spectra simultaneously with other stations. The Concordia station is essential because it combines low geomagnetic cutoff rigidity (no geomagnetic shielding) and high altitude. Finally, a metrological reference is based on an instrument in Toulouse, France. Figure 1 shows detailed characteristics of the Concordia station and Pic-du-Midi observatory, including the geographical location, the cutoff rigidity, and spectrometer characteristics.
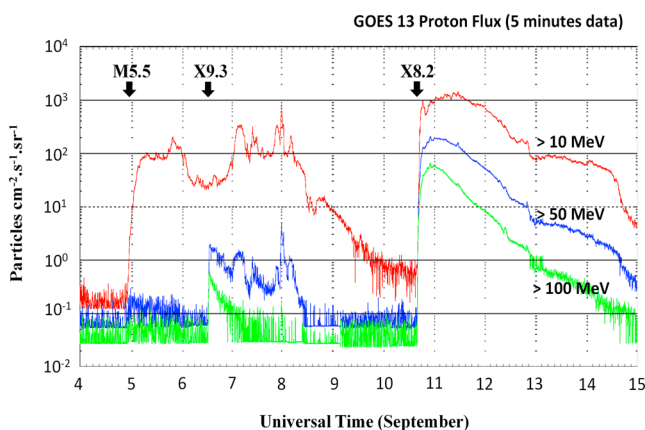

Figure 4. Five-minute averaged integral proton fluxes (in pfu = protons/cm^2·s·sr) as measured by a GOES satellite for each of the energy thresholds: >10, >50, and >100 MeV, from 04 to 15 September 2017. Vertical arrows indicate three analyzed solar events with M5.5, X9.3, and X8.2 flares. Figure issued from NOAA.
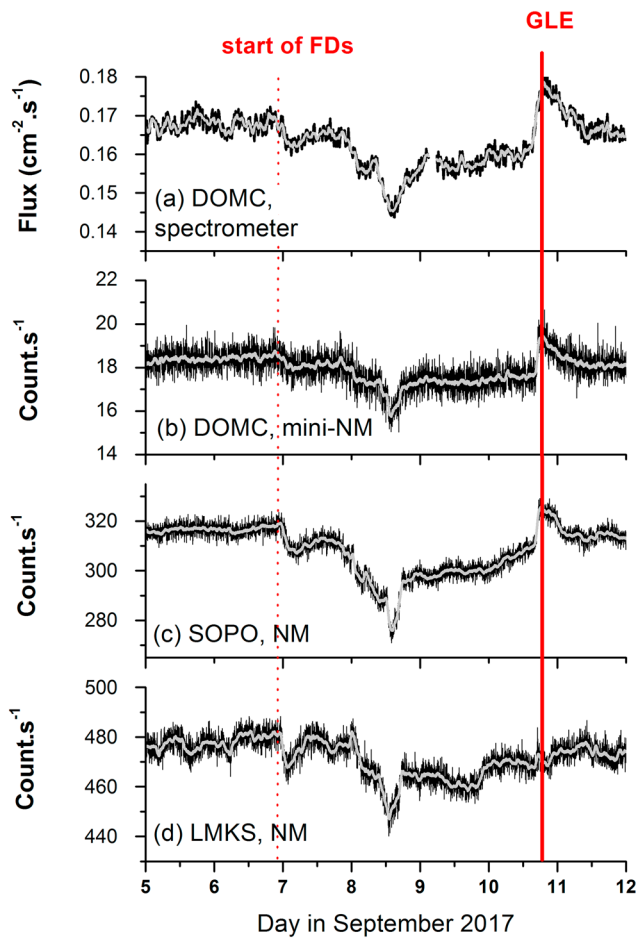
Figure 5. Count rates measured with neutron monitors during solar events occurring in September 2017, (a) DOMC using spectrometer, (b) DOMC, (c) SOPO, and (d) LMKS using NMs. Data are averaged over 2 min (black) and 1 hr (gray) for NMs, and 15 min (black) and 1 hr (gray) for the neutron spectrometer.

2.2. Environmental and Systematic Effects on Measurements

Several parameters can influence the measurement, in particular, the atmospheric pressure, the hydrometric environment close to the instrument (snowfall), and the atmospheric water vapor (Ruffalo et al., 2016). Data on air pressure are recorded to correct the count rates to a reference pressure. Water vapor contents were recorded in Concordia station in the framework of the H_2O Antarctica Microwave Stratospheric and Tropospheric Radiometers project (Ricaud, Gabard, Derrien, Chaboureau, et al., 2010). The radiometer uses spectral information in the microwave bands 51–59 GHz (V-band, lower frequency wing of the oxygen line) and 169–197 GHz (G-band, strong water vapor line, centered at 183.3 GHz) to derive accurate tropospheric profiles of temperature and low humidity. For temperature profiling, the pressure-broadened oxygen line shape is evaluated, while the strong water vapor line allows for the profiling of very low humidity with an IWV amount of <2 kg/m^2 (or <2 mm in precipitable water units). A statistical approach is used to calculate the profiles from the brightness temperatures measured by the radiometer, which provide a set of temperature and humidity data points as a function of altitude.

Among all these contributions, the atmospheric water vapor dominates the ground cosmic ray variations within the first few hundred meters above the ground (Rosolem et al., 2013). Conditions of soil moisture have a major influence on the neutron flux; that is, the neutron flux for a given value of water vapor content reduced when the soil moisture decreases. Given the absence of precipitation during the studied time period (1–13 September 2017, at the Pic du Midi and Concordia), the impact of the change in soil moisture can be neglected, contrary to the water vapor content variations.

Two contributions were considered to correct count rate data, the air pressure and the water vapor. Thus, corrected count rate by air pressure is given by the equation (1):
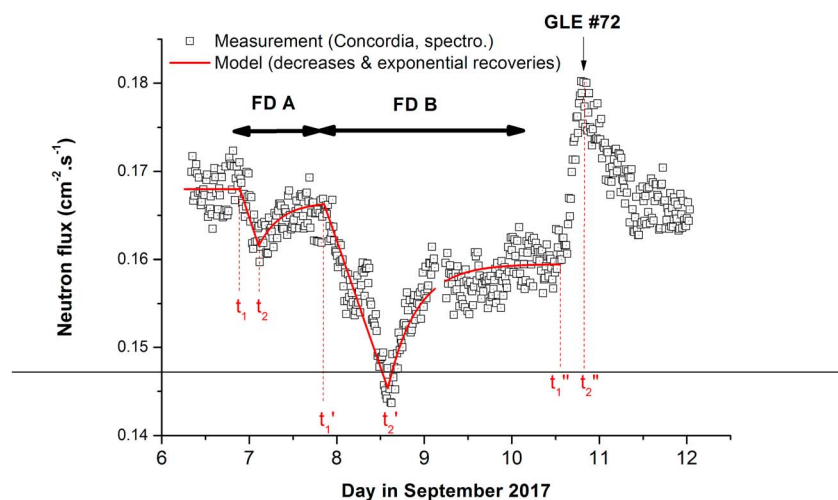

Figure 6. Total neutron fluence rate measured at Concordia station using neutron spectrometer and during solar events occurring in September 2017. Two FDs (named A and B) are observed and adjustments were added and best fit parameters are presented in Table 1.

Table 1
FD Characteristics (Timing and Amplitudes A_{FD})

	FD A	FD B
t_1	06/09/2017 23:08:00	07/09/2017 19:54:00
t_2	07/09/2017 04:31:00	08/09/2017 06:17:00
A_{FD}	3.4%	11.3%

$$C_{P,\text{corr}} = C.e^{-\beta(P_0 - P)} \tag{1}$$

where β is the barometric coefficient (% hPa^{-1}) empirically determined and C_{corr} is the corrected count rates. The β factor, equals to 7.1×10^{-3} hPa^{-1}, was empirically determined in a previous work (Leuthold et al., 2007). As described in (Rosolem et al., 2013), the atmospheric humidity in the count rate data is taken into account using a single scaling factor C_{WV} determined by simulations (Rosolem et al., 2013):

$$C_{\text{WV,corr}} = C \times (1 + 0.0143 \times \Delta \text{IWV}) \tag{2}$$

where ΔI_{WV} corresponds to the difference of the integrated vapor density value with the reference value on the day of the calibration. Concordia environment is well known and stable over time (low precipitation levels). It is one of the driest and coldest places over the world with precipitable water or integrated water vapor (IWV) less than 1 kg/m^2 over the year reaching less than 0.1 kg/m^2 in winter (Ricaud et al., 2015). The atmosphere is considered in the dome C when the absolute humidity reaches 0.3 g/m^3, which is very low compared to values observed in typical moist conditions (i.e., 20 g/m^3). Figure 2 presents (a) the atmospheric pressure, (b) the IWV parameter (water vapor integrated along the vertical from the surface to the tropopause), and (c) the uncorrected/corrected hourly count rate (9″ lead sphere) recorded in Concordia during solar events. Corrected rates are presented considering pressure and pressure/vapor impacts. The water vapor density is plotted for several altitudes.

As stated above, the data show that the Concordia environment can be therefore considered extremely dry. As shown in a previous work (Rosolem et al., 2013), for low atmosphere water vapor content and IWV (in the order of few tenths of g/m^3 or kg/m^2 for absolute humidity and IWV, respectively), environmental or systematic effects on fast neutrons are negligible (i.e., a few tenths of a percentage) while they are significant for low-energy neutrons (epithermal and thermal).

The situation is different in the Pic du Midi because the atmospheric vapor content and their variations are significant (Ricaud, Gabard, Derrien, Attié, et al., 2010), involving environmental or systematic effects on CR measurements in the orders of 10%. Indeed, seasonal analyses show that an extreme variability of the atmosphere water vapor content can be noted, from extremely dry conditions in winter to extremely wet conditions in summer. The order of magnitude of the absolute humidity are in the range from low values to 12 g/m^3, which according to analyses proposed in Rosolem et al. (2013) has potentially important impact on fast neutrons. Meteorological measurements conducted in the Pic du Midi during the September 2017 period are less comprehensive than those of Concordia. Thus, the relative humidity H and the temperature T records allow to determine the surface water vapor pressure E_W using equation (3):

$$E_W = 4.585 \frac{H}{100} e^{\left(\frac{17.62 \times T}{T + 243.12}\right)} \tag{3}$$

Figure 3 presents (a) the atmospheric pressure, (b) the surface water vapor pressure recorded during this period, and (c) uncorrected and corrected by pressure hourly count rates. The data analysis shows that the relative humidity and surface water vapor surface values are typical of summer conditions and their variations are relatively low.

To conclude, it is obvious that neutrons can be significantly impacted by environmental variations. Water vapor data might be considered in CR analyses, taking into account a water vapor correction using scaling factor deduced from calibrations. FDs and GLE occurred in September 2017 appear to be significant compared to the environmental influences.
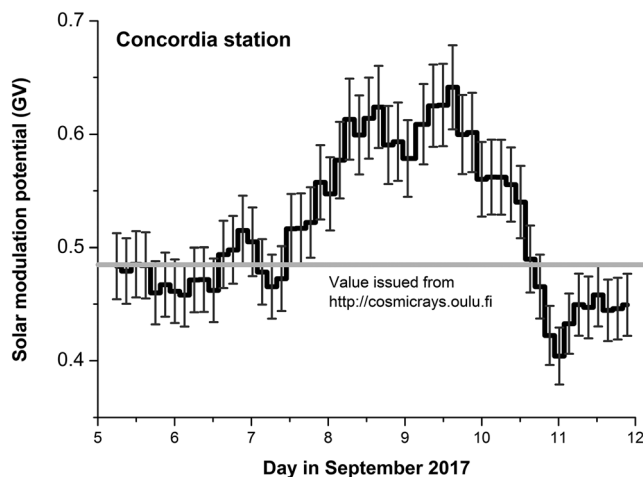

Figure 7. Solar modulation potential in GV during the September 2017 solar event, reconstructed from the neutron spectrometer data, Concordia station.
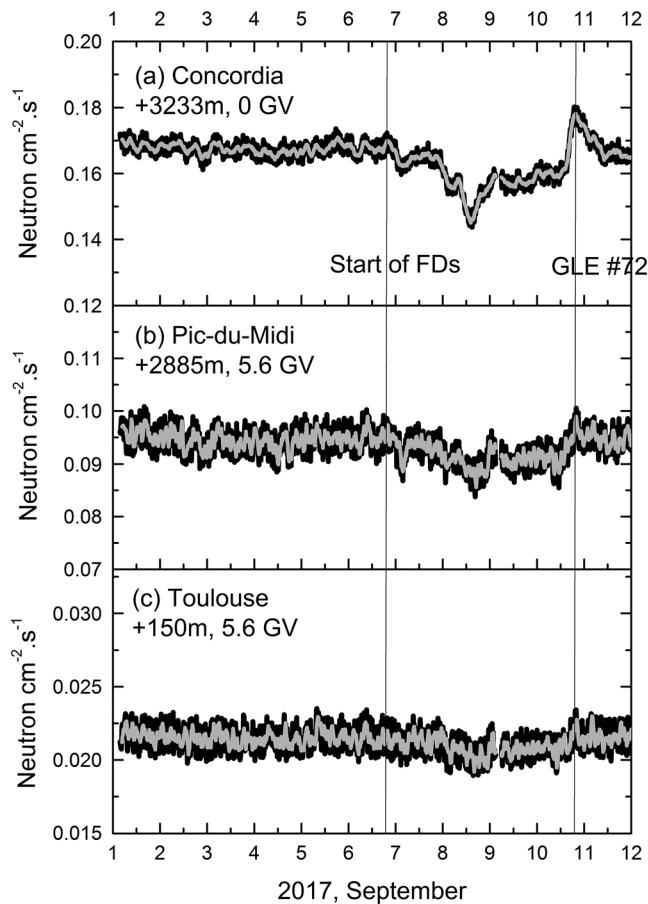
Figure 8. Total neutron flux measured at the (a) Concordia station, (b) Pic-du-Midi observatory, and (c) the French aerospace laboratory (located in Toulouse) during September 2017. The integration times of count rates are 5 min (black point) and 1 hr (gray point), respectively.

3. Description of the September 2017 Solar Event

In September 2017, the Sun was very active inducing solar flares during the first days of the month. After a series of major flares including 27 M-class and 4 X-class flares, the solar active region had produced an X9.3 flare on 6 September, which is the most powerful in the last 10 years (CME-List, https://cdaw.gsfc.nasa.gov/CME_list/halo/halo.html). The solar activity decreased on 9 and 10 September. Bright gamma-ray emission from the X8.2 class solar flare was recorded on 10 September 2017 by the Large-Area Telescope (Glast, https://www-glast.stanford.edu/) and Fermi Gamma-ray Space Telescope (Atwood et al., 2009). This flare was characterized by a SEP event with high-energy particles, producing nuclear cascades in the atmosphere and detected on the ground. This flare was the second GLE (#72) of the current solar cycle.

Data presented in Figure 4 are issued from NOAA; they correspond to 5-min-average integral proton fluxes measured from 04 to 15 September 2017 by a GOES satellite for each of the energy thresholds: >10, >50, and >100 MeV, from 04 to 15 September 2017. Vertical arrows indicate three analyzed solar events with M5.5, X9.3, and X8.2 flares. In the point of view of the geomagnetic field, quiet to minor storm levels occurred on 04 September while quiet to active levels on 05–06 September. Late on 06 September, the first of two CMEs were observed. The first CME (associated with the M5 flare) was observed on Earth at 23:08:00 UT 06 September 2017, and it could be seen in the LASCO coronagraph (https://www.swpc.noaa.gov/products/lasco-coronagraph) already on 4 September at about 19:10:00 UT. Total interplanetary field increased to 16 nT at 23:24:00 UT and solar velocity increased to a maximum of 610 km/s at 06 September 2017 23:09:00 UT. Then, when the second CME occurred, solar velocity increased to a maximum of 842 km/s at 08 September 2017 08:48:00 UT while total magnetic field increased to a maximum of 34 nT at 07 September 2017 22:54:00 UT.

Energetic particles are continuously monitored by ground-based NMs. Data provided by the NM database (NMDB; http://nmdb.eu) and the neutron spectrometer operated in the Concordia station are presented in Figure 5. Count rates or flux are given between 5 and 12 September 2017, and include (a) DOMC (*Concordia station*, Antarctica) using neutron spectrometer, (b) DOMC, (c) SOPO (*South Pole station*, Antarctica), and (d) LMKS (*Lomnicky Stit*, Slovakia) using NMs. Solar events are characterized first by FDs from 6 September, and then a GLE occurred on 10 September during the late recovery of an FD. The increase in CR intensity during the GLE began at about 16:00:00 UT. The increase was significant for the DOMC and SOPO data (Mishev et al., 2018), while negligible for the LMKS station which is located in Slovakia and characterized by a higher cutoff rigidity of 3.84 GV.

In Figure 5, two FDs are distinguishable, the second being a classical two-step FD. Solar events are particularly observed in the Antarctica region because the cutoff rigidity is very low. The Concordia station is attractive because a mini-NM and a spectrometer have monitored the solar flare simultaneously, allowing a coupled analysis of neutron fluxes and spectra. Figure 5 shows the neutron count rate and flux recorded during solar event. The FD and the GLE are perfectly observed with both instruments, and the timing is relevant.

4. Analyses of FDs and GLE Based on Neutron Fluxes

4.1. FD Analyses of the September 2017 Solar Event

A FD can be described by several phases based on coupled mechanisms due to shock and ejecta phases (Cane, 2000). The decrease phase starts with the arrival of shock at magnetopause and when the Earth
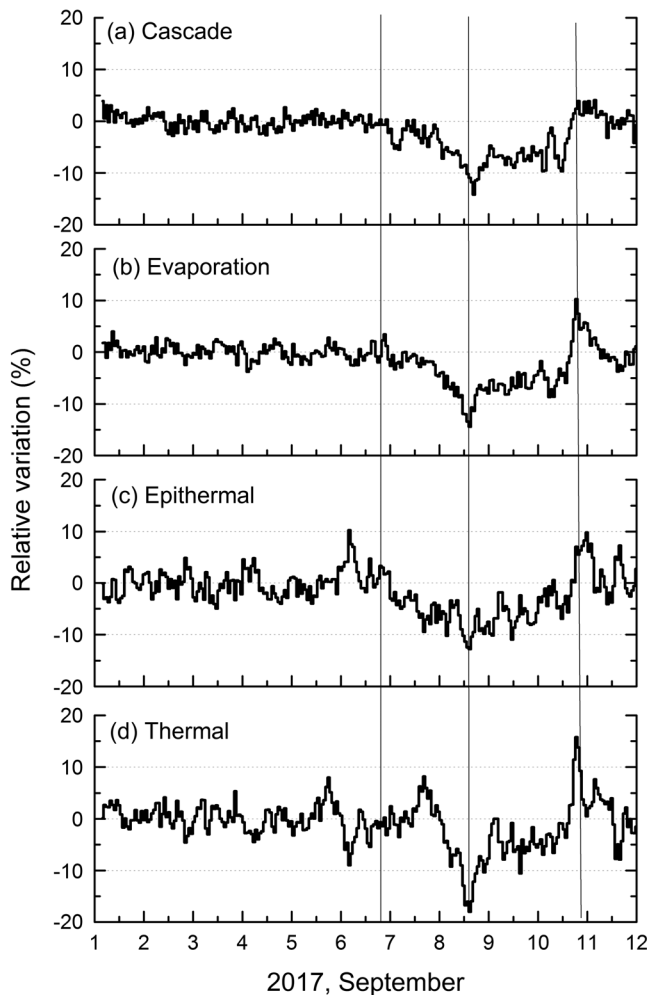
Figure 9. Relative variations (in %) for the cascade, evaporation, and epithermal and thermal neutrons (Concordia, from 1 to 12 September).

enters a region of reduced particle flux. The preincrease in cosmic ray intensity (typically 2–3%) can be associated to the onset of FDs. The preincrease is usually of very short duration (i.e. few hours), although it may also extend to longer periods. A FD recovery phase occurs and can be composed by rapid and gradual steps. This phase is classically described using single exponential function fitting and characterized by a time constant (Jamsen et al., 2007; Sidhu, 2017).

Thus, to describe FDs recorded during the September 2017 event, three stages can be applied. The first stage is before the instants t_1 (i.e., before the disturbance), and the total flux is considered in a stationary state. A low preincrease is observed during this stage. The second step is characterized by a fast decrease of neutron flux at ground from the instants t_1 to t_2, and quantifies the FD amplitude, named A_{FD}. The third step corresponds to an exponential recovery to the quiet conditions. The amplitude A_{FD}, derived from equation (3), depends on the CR modulation and the cutoff rigidity associated to the geomagnetic latitude. φ_D corresponds to the energy-integrated neutron flux in the energy domain D (thermal, epithermal, evaporation, cascade, or total).

$$A_{\mathrm{FD}} = \frac{|\phi_D(t_1) - \phi_D(t_2)|}{\phi_D(t_1)} \qquad (4)$$

Concerning the event of September 2017 and basing on neutron spectrum measured in Concordia station, two FDs can be identified (referenced A and B) and are presented in Figure 6. Table 1 provides details for timing and amplitude. The FD identified as B is composed by diurnal variations due to the anisotropy and superposed on the recovery step.

The FD identified as B is a typical classical multistep FD (Bhaskar et al., 2016); the amplitudes of steps are in the order of 3.4% and 11.3%, respectively. It is well accepted that the classical multistep FD represents sheath and magnetic cloud/ejecta signature (Cane, 2000). However, by associating steps, the amplitude is in the order of 12.8% in Concordia, classifying this event as one of the most interesting of the current solar cycle. The fact that a GLE occurred during this event gives it a significant interest.

B. Solar modulation potential reconstruction during the solar events of September 2017.

Previous analyses (Cheminet, Hubert, Lacoste, Maurin, et al., 2013; Ghelfi et al., 2017; Hubert, Li Cavoli, et al., 2015; Maurin et al., 2015; Usoskin et al., 2005; Usoskin et al., 2011) have shown a possibility to characterize neutron measurements (NMs or spectrometer) by the solar potential ɸ(t) depending on the Sun's activity in the context of the force-field approximation. Calculations using the Force-Field approximation and the air-shower modeling allows to investigating the time evolution of ɸ(t). The solar modulation potential is a modeling parameter which is based on ground measurements and depends on the choice of the local interstellar spectrum (LIS) model. In the past LIS spectra have been established in many ways (Burger et al., 2000; Mrigakshi et al., 2012) and the *Burger-Usoskin* LIS spectrum was considered in this work (Usoskin et al., 2005). However, the physical interpretation of the modulation potential is not straightforward during periods of active Sun (Usoskin et al., 2011) and requires more refined physical analyses.

The standard methods to determine ɸ(t) are based on NMs, whose advantages are the existence of an worldwide network, the efficient integration time (typically $t_{int} > 1$ min) and the high coverage of the geomagnetic latitudes using one of the several yield functions calculated in the literature (Clem & Dorman, 2000; Flückiger et al., 2007; Mangeard et al., 2016; Mishev et al., 2013; Nagashima, 1990). As previously described, ɸ(t) depend on models for the *Berger-Usoskin* LIS spectrum (Mrigakshi, 2012). Monthly averaged
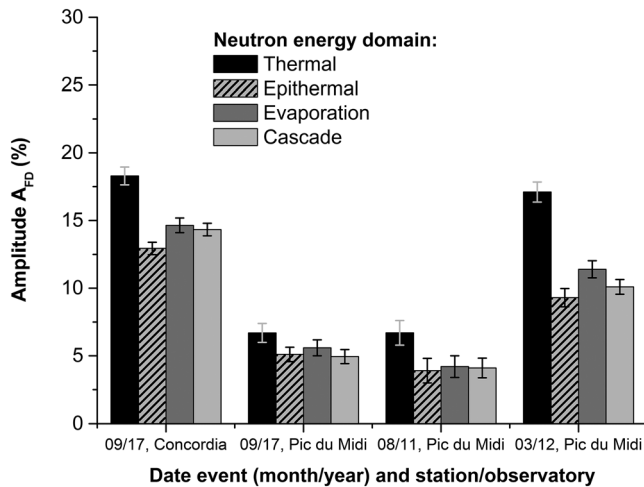
Figure 10. Forbush decrease amplitude A_{FD} from neutron spectrometer operated at Pic-du-Midi observatory and during solar events occurring in August 2011 and March 2012. Results concerning the September 2017 event recorded in the Pic du Midi and in Concordia were added. Uncertainties were calculated considering hourly count rate.

modulation parameters from 1951 are available (Herbst et al., 2010; Usoskin et al., 2005; Usoskin et al., 2011), using several LISs and several NMs. An alternative (Cheminet, Hubert, Lacoste, Maurin, et al., 2013; Hubert, Li Cavoli, et al., 2015) consists in using cascade neutron fluxes issued from neutron spectrometers, and relying on ATMORAD model (Hubert, Li Cavoli, et al., 2015) to deduce the modulation potentials in the Force-Field approximation in this period (assuming a LIS flux). This approach was compared to an independent determination using NM count rates from the Oulu CR station (*Oulu*), and they show a good agreement during solar events occurred in March 2012 (Hubert, Li Cavoli, et al., 2015). This methodology has allowed us to characterize the observed FD, whose amplitude is linked to the effective galactic cosmic ray modulation.

Figure 7 presents the solar modulation potential in GV, deduced from neutron spectrometer data in the Concordia station during the September 2017 solar events. The time integration was considered as 6 hr and only cascade neutrons spectra were used. The monthly values of the modulation parameter reconstructed from the ground-based CR data, using the procedure described in Usoskin et al. (2017) and considering that the LIS corresponds to Vos and Potgieter (2015), are in the order of 0.5 GV during September 2017. The CR spectrum during a strong solar event can be too complex to be well described by a single modulation parameter, mainly due to an additional solar component in the spectrum.

4.2. Cross Analyses of Neutron Fluxes

Three neutron spectrometers recorded the September 2017 solar event. Figure 8 presents the neutron flux dynamic measured simultaneously at (a) Concordia station, (b) Pic-du-Midi observatory, and (c) the French Aerospace laboratory located in Toulouse. Two integration times were considered, 5 min (black points) and 1 hr (gray points), respectively. The evolution of the flux at the Concordia station was presented first in Figure 5 and detailed in Figure 6. The data analyses indicate a decrease in the order of 11% of the amplitude A_{FD}. In comparison, during solar events occurring in March 2012 and analyzed using the same spectrometer, a decrease of about 10% was observed, which is quite similar to the September 2017 event.

5. Analyses Based on Neutron Spectrum

5.1. Analyses of Measured Cosmic Ray-Induced Neutron Spectra

The neutron energy domain ranges from 10 meV to several GeV and can be divided in four domains reflecting physical mechanisms such as thermalization, evaporation, and direct high-energy interactions. The thermal region corresponds to the neutron energies below 0.5 eV, and the intermediate energy domain from 0.5 eV to 0.1 MeV is defined as the epithermal neutrons. Then, the evaporation and the cascade regions are defined from 0.1 to 20 MeV and above 20 MeV, respectively.

Figure 9 presents the relative variations for each energy domain obtained from the neutron spectrometer in Concordia station. References of relative variations correspond to the average fluxes relative to the quiet period before solar events (01 to 06 September). The variability of relative variations is more significant for thermal and epithermal domains, probably because environmental or systematic effects (water vapor content variations). Complementary contributions could be related to the selected Bonner spheres which favor fast and high-energy neutron detections (i.e., 8″, 12″, 9″L and 8″W).

Despite these systematic fluctuations, FDs and the GLE impacts appear to be significant to analyze each energy domain. Thus, epithermal, evaporation, and cascade domains are disturbed in a comparable way during FD events, in the order of 12 to 15%. However, the thermal domain is significantly more impacted. Analyses of the GLE indicate that cascade neutrons is enriched by about 4% while thermal, epithermal, and evaporation domains increase by 10 to 14%. Such differences are not attributed to environmental variations, implying a mechanisms inherent to the GLE properties and mechanisms.
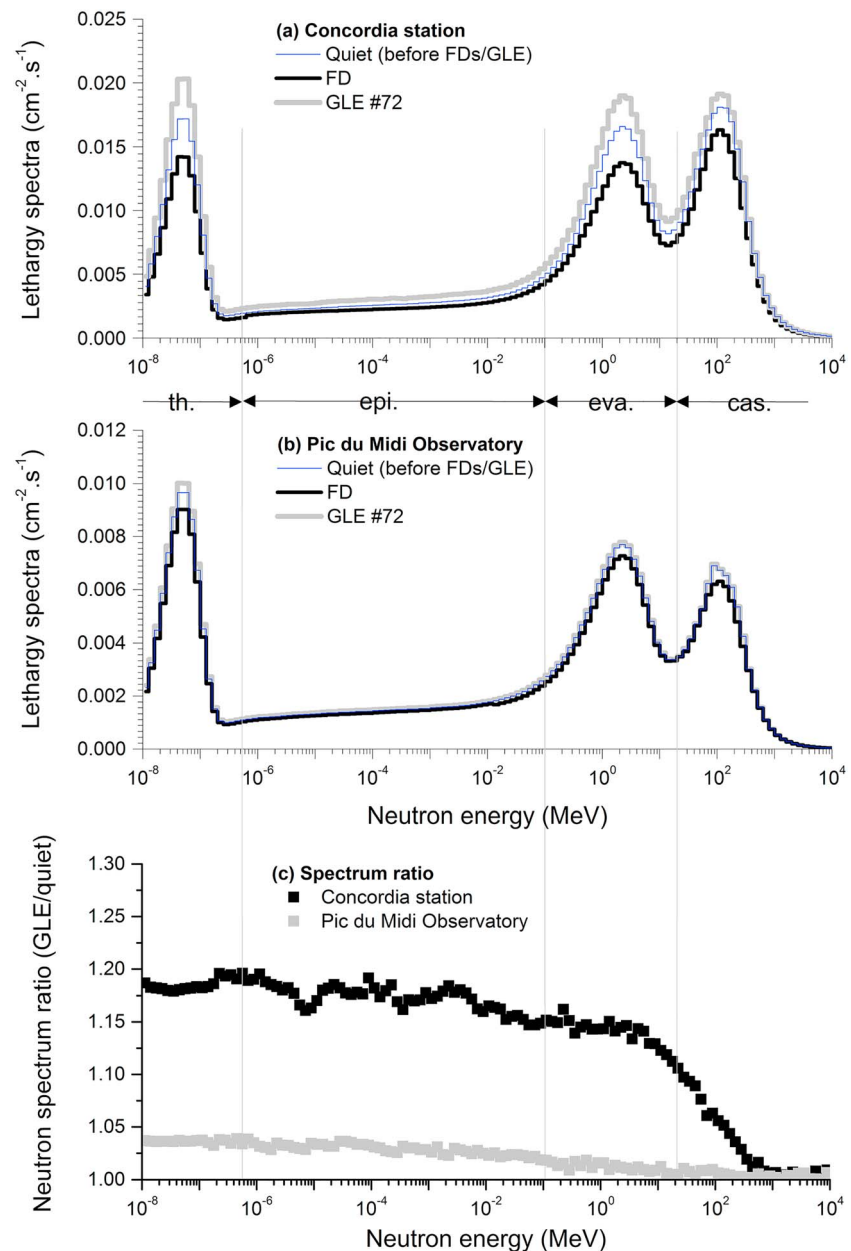
Figure 11. Lethargic spectra measured at the (a) Concordia station and (b) Pic du Midi observatory. Experimental curves concern the preevent spectrum, the spectrum when the disturbance of the FD is maximal (08 September 2017, 14:02:12 UT), and the spectrum during the GLE (10 September 2017, 18:58:18 UT). (c) Ration of the neutron spectrum during the active period (GLE) to that during the quiet period, for the Concordia station and the Pic du Midi observatory. Neutron energy domains are added to correlate the impacted energy.

Significant FD events occurring in August 2011 and March 2012 were recorded by the neutron spectrometer operated in the Pic du Midi observatory (Cheminet, Hubert, Lacoste, Boscher, et al., 2013; Hubert, Pazianotto, et al., 2016). Figure 10 presents the amplitude A_{FD} measured during these previous events as well as data obtained during the September 2017 event at the Pic du Midi and Concordia station. Average value and uncertainties were calculated considering 2-hourly count rate, allowing to mitigate the impact of environmental effects (mainly for the Pic du Midi) on average values. A 2-hr integration time is justified by the FD time characteristic (not applicable in the case of GLE). Analyses of previous events provide similar trends, for example, a certain homogeneity of amplitude for epithermal, evaporation, and cascade domains, while thermal energies are more impacted. It is
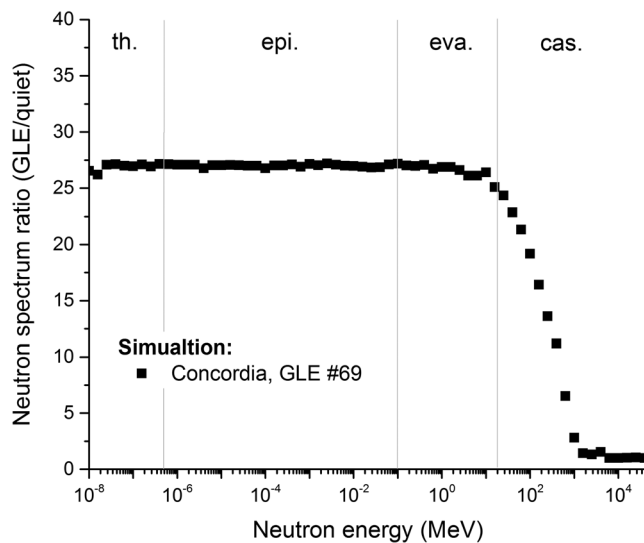
Figure 12. Ratio of the neutron spectrum during the active period (GLE) to that during the quiet period, considering simulations of the Concordia and the GLE #69 characteristics.

not simple to physically explain this phenomenon, but it could be explained due to the thermalization process of the scene of albedo neutrons which favor the reinforcement of the thermal energies (Rühm et al., 2009; Hubert, 2017a; Hubert, Pazianotto, et al., 2016).

The neutron spectrometry also makes it possible to represent the lethargy spectrum, that is, $E \times \varphi(E)$ in unit cm²/s, and to study its variations during the solar flare event. Spectra obtained using an integration time of 30 min were presented in Figure 11a; the time reference corresponds to the center of the interval. Three lethargic spectra are considered: the preevent spectrum (05 September 2017, 14:02:00 UT), the spectrum when the disturbance of the FD is maximal (08 September 2017, 14:02:00 UT), and the spectrum during the GLE (10 September 2017, 18:58:00 UT). Referring to the peak values, the thermal, epithermal, and evaporation neutron populations increase more than cascade neutrons during the GLE. The thermal peak presents a change in amplitude that is resulted of changing of the evaporation neutron population. Evaporation neutrons are moderated in the environment producing thermal neutrons and, than, the increasing thermal neutrons are directly impacted by the increasing of evaporation neutron component. Although the Pic-du-Midi data are less accurate because of the 30-min integration time, Figure 11b presents lethargy spectra according to the same method. It is interesting to note that trends are very similar, that is, a significant neutron enrichment in thermal, epithermal, and evaporation domain, while a low increase of cascade neutrons is observed.

To more effectively analyze these differences, the ratio of the neutron spectrum during the active period (GLE) to that during the quiet period are presented in Figure 11c, considering the Concordia station and the Pic du Midi Observatory. Neutron energy domains are added to easily identify the impacted energy. Thus, Figure 11 shows the relatively weak increase of cascade neutrons during a GLE, while other energy domains are impacted in similar orders of magnitude, from 15 to 20%.

5.2. Preliminary Analysis Based on Air Shower Modeling

The purpose of this section is to explain qualitatively the analysis based on Figure 11c using atmospheric shower simulations of solar energetic particles (Hubert & Aubry, 2017a; Hubert & Cheminet, 2015). Nevertheless, SEP spectrum of GLE #72 was not described while SEP characteristic parameters for some significant events were reconstructed (Buetikofer & Fueckiger, 2013; Mishev & Usoskin, 2016; Plainaki et al., 2007; Raukunen et al., 2018). Analyses concern the GLE #69 (Makhmutov et al., 2008; Mironova et al., 2012; Miyasaka et al., 2005) which has the advantage of being the most recent large-intensity event. Moreover, GLE #69 was monitored by most operational NMs. Indeed, the approach proposed by Plainaki et al. described the GLE #69 occurred on 20 January 2005 including differential spectra and anisotropy functions for different times. If it is not possible to assess the event-integrated fluence, this approach provides the instantaneous spectrum characteristics when the disturbance is utmost. Figure 12 presents the ratio of the neutron spectrum between the active and the quiet period, considering the Concordia station and the GLE #69.

As observed experimentally for the GLE #72, the cascade domain is low impacted during the active period, while other domains are impacted in similar orders of magnitude. Both solar events are not directly comparable because their characteristics are different (rigidity spectrum, anisotropy, and dynamics). Nevertheless, solar CR can reach up to 1–10 GeV/n during typical GLE, more exceptionally 10–30 GeV/n for extreme events (as GLE #5 occurring in 23 February 1956; Belov et al., 2005). To conclude, simulation results for GLE #69 in Figure 12 look similar to the Concordia data for GLE #72 (Figure 11c), confirming that the relatively weak increase of cascade neutrons during a GLE is reasonably explained by the physics of atmospheric showers from SEP particles, which are much less energetic than typical galactic cosmic rays.

6. Conclusion

In this paper, an analysis of neutron spectrum variations during solar event implying a series of FDs and the GLE #72 (September 2017) was presented. Investigations are based on data recorded by neutron spectrometers located at the Pic-du-Midi Observatory and the Concordia station (low cutoff rigidity and high altitude). Thanks to the CHINSTRAP project, neutron spectra were recorded since December 2015, including periods during solar events. Neutron spectra dynamics can be investigated in the framework of long-term (Hubert, Pazianotto, et al., 2016; i.e., CR seasonal variations) and short-term (solar events) analyses.

Analyses were presented for solar events occurring in September 2017, distinguishing FD and GLE events. Concerning FDs, investigations are compared with analyses performed for previous FDs (August 2011 and March 2012).

Spectral analyses focused on the differences observed between a quiet time, the maximum FD and during the GLE. During the GLE event, thermal, epithermal, and evaporation neutrons increase relatively uniformly while cascade neutrons are not impacted. This was found in data from both Concordia and Pic-du-Midi for 10 September 2017. Simulations of GLE #69 impacts, for which it is possible to describe the SCR contribution, were performed and qualitatively confirm these trends.

References

Atwood, W. B., Abdo, A. A., Ackermann, M., Althouse, W., Anderson, B., Axelsson, M., et al. (2009). The large area telescope on the Fermi gamma-ray space telescope mission. *The Astrophysical Journal*, *697*(2), 1071–1102. https://doi.org/10.1088/0004-637X/697/2/1071

Belov, A. V., Eroshenko, E. A., Mavromichalaki, H., Plainaki, C., & Yanke, Y. G. (2005). Solar cosmic rays during the extremely high ground level enhancement on 23 February 1956. *Annales Geophysicae*, *23*(6), 2281–2291. https://doi.org/10.5194/angeo-23-2281-2005

Bhaskar, A., Vichare, G., Arunbabu, K. P., & Raghav, A. (2016). Role of solar wind speed and interplanetary magnetic field during two-step Forbush decreases caused by interplanetary coronal mass ejections. *Astrophysics and Space Science*, *361*(7), 242–255. https://doi.org/10.1007/s10509-016-2827-8

Buetikofer, R., & Fueckiger, E. O. (2013). Differences in published characteristics of GLE60 and their consequences on computed radiation dose rates along selected flight paths. *Journal of Physics: Conference Series*, *409*. https://doi.org/10.1088/1742-6596/409/1/012166

Burger, R., Potgieter, M., & Heber, B. (2000). Rigidity dependence of cosmic ray proton latitudinal gradients measured by Ulysses spacecraft: Implications for the diffusion tensor. *Journal of Geophysical Research*, *105*, 27,447–27,455. https://doi.org/10.1029/2000JA000153

Cane, H. V. (2000). Coronal mass ejections ands Forbush decreases. *Space Science Reviews*, *93*(1/2), 55–77. https://doi.org/10.1023/A:1026532125747

Cheminet, A., Hubert, G., Lacoste, V., & Boscher, D. (2013). Measurements and Monte-Carlo simulations of the spectral variations of the cosmic-ray-induced-neutrons at the Pic-du-Midi over a 2-y period. *Radiation Protection Dosimetry*, *161*(1–4), 284–289. https://doi.org/10.1093/rpd/nct330

Cheminet, A., Hubert, G., Lacoste, V., Maurin, D., & Derome, L. (2013). Cosmic-ray solar modulation and Forbush decrease analyses based on atmospheric neutron spectrometry at mountain altitude and GEANT4 simulations of extensive air showers. *Journal of Geophysical Research: Space Physics*, *118*, 7488–7496. https://doi.org/10.1002/2013JA019166

Cheminet, A., Lacoste, V., Gressier, V., Hubert, G., Martin, A., & Pépino, M. (2012). Characterization of the IRSN neutron multisphere spectrometer (HERMEIS) at European standard calibration fields. *IOP Science Journal of Instrumentation*, *7*, 1–17.

Clem, J. M., & Dorman, L. I. (2000). Neutron monitor response functions. *Space Science Reviews*, *93*(1/2), 335–359. https://doi.org/10.1023/A:1026508915269

Dorman, L., Gushchina, R., Shei, M.A., Smart, D.F. (1972). Effective cut-off rigidities of cosmic rays. *Technical Report*.

Dunai, T. J. (2015). *Cosmogenic Nuclides: Principles, Concepts and Applications in the Earth Surface Sciences*. New York: Cambridge University Press.

Eroshenko, E.P., Velinov, A., Belov, V., Yanke, E., Mishev, A., Tassev, Y. (2008). Relationships between cosmic ray neutron flux and rain flows. *21st European Cosmic Ray Symposium*, 127-131.

Flückiger, E. O.; Moser, M. R.; Pirard, B.; Bütikofer, R.; Desorgher, L. A. (2007). Parameterized neutron monitor yield function for space weather applications. Proceedings of ICRC.

Forbush, S. E. (1937). On the effect in cosmic-ray intensity observed during the recent magnetic storm. *Physical Review*, *51*(12), 1108–1109. https://doi.org/10.1103/PhysRev.51.1108.3

Ghelfi, A., Maurin, D., Cheminet, A., Derome, L., Hubert, G., & Melot, F. (2017). Neutron monitors and muon detectors for solar modulation studies: 2. φ time series. *Advances in Space Research*, *60*(4), 833–847. https://doi.org/10.1016/j.asr.2016.06.027

Gleeson, L., & Axford, W. (1968). Solar modulation of galactic cosmic rays. *The Astrophysical Journal*, *154*, 1011–1027.

Goldhagen, P., Clem, J., & Wilson, J. (2004). The energy spectrum of cosmic-ray induced neutrons measured on an airplane over a wide range of altitude and latitude. *Radiation Protection Dosimetry*, *110*(1-4), 387–392. https://doi.org/10.1093/rpd/nch216

Grieder, P. K. F. (2001). *Cosmic Rays at Earth: Researcher's Reference Manual And Data Book*, (1st ed.p. 1093). Amsterdam: Elsevier.

Hatton, C. J., & Carmichae, L. H. (1964). Experimental investigation of the NM-64 neutron monitor. *Canadian Journal of Physics*, *42*, 2443–2473.

Herbst, K., Kopp, A., Heber, B., Steinhilber, F., Fichtner, H., Scherer, K., & Matthiä, D. (2010). On the importance of the Local Interstellar Spectrum for the Solar Modulation Parameter. *Journal of Geophysical Research*, *115*, D00I20. https://doi.org/10.1029/2009JD012557

Hubert, G. (2016). Analyses of cosmic ray induced-neutron based on spectrometers operated simultaneously at mid latitude and Antarctica high-altitude stations during quiet solar activity. *Astroparticle Physics Journal*, *83*, 30–39. https://doi.org/10.1016/j.astropartphys.2016.07.002

Hubert, G. (2017a). Ground albedo neutron impacts to seasonal variations of cosmic-ray-induced neutron in medium geomagnetic latitude and Antarctica: Impacts on soft error rate. *IEEE Transactions on Nuclear Science*, *64*(1), 622–629. https://doi.org/10.1109/TNS.2016.2614540

Hubert, G. (2017b). First eighteen months of simultaneously measurements of the energy spectrum of cosmic-ray induced neutrons on the Pic-du-Midi Observatory and the Concordia station in Antarctica. *Proceedings of ICRC*.

Hubert, G., Artola, L., & Regis, D. (2015). Atmospheric radiation impacts on the soft error sensitivities along the VLSI trend of bulk, FDSOI and FinFET technologies. *Integration, the VLSI Journal*, *50*, 39–47. https://doi.org/10.1016/j.vlsi.2015.01.003

Hubert, G., & Aubry, S. (2017a). Atmospheric cosmic-ray variation and ambient dose equivalent assessments considering ground level enhancement thanks to coupled anisotropic solar cosmic ray and extensive air shower modeling. *Radiation Research*, *188*(5), 517–531. https://doi.org/10.1667/RR14761.1

Hubert, G., & Aubry, S. (2017b). Analysis of solar and galactic cosmic rays induced atmospheric ionizing radiation: Impacts for typical transatlantic flights and Antarctica environment. *JSM Environmental Science & Ecology*, *5*(3), 1050.

Hubert, G., & Cheminet, A. (2015). Radiation effects investigations based on atmospheric radiation model (ATMORAD) considering GEANT4 simulations of extensive air showers and solar modulation potential. *Radiation Research*, *184*(1), 83–94. https://doi.org/10.1667/RR14028.1

Hubert, G., Federico, C. A., Pazianotto, M. T., & Gonzales, O. L. (2016). Long and short-term atmospheric radiation analyses based on coupled measurements at high altitude remote stations and extensive air shower modeling. *Astroparticle Physics Journal*, *74*, 27–36. https://doi.org/10.1016/j.astropartphys.2015.09.005

Hubert, G., Li Cavoli, P., Federico, C., Artola, L., & Busto, J. (2015). Impact of the radial ionization profile of proton on SEU sensitivity of nanoscale SRAMs. *IEEE Transactions on Nuclear Science*, *62*(6), 2837–2845. https://doi.org/10.1109/TNS.2015.2496238

Hubert, G., Pazianotto, M. T., & Federico, C. A. (2016). Modeling of ground albedo neutrons to investigate seasonal cosmic-ray-induced neutron variations measured at high-altitude stations. *Journal of Geophysical Research: Space Physics*, *121*, 186–201. https://doi.org/10.1002/2016JA023055

Hubert, G., Trochet, P., Riant, O., Heinz, P., & Gaillard, R. (2004). A neutron spectrometer for avionic environment investigations. *IEEE Transactions on Nuclear Science*, *51*(6), 3452–3456. https://doi.org/10.1109/TNS.2004.839130

Hubert, G., Velazco, R., Frederico, C., Cheminet, A., Silva-Cardenas, C., Caldas, L. V. E., et al. (2013). Continuous high-altitude measurements of cosmic ray neutron and SEU/MCU at various locations: Correlation and analyses based-on MUSCA-SEP3. *IEEE Transactions on Nuclear Science*, *60*(4), 2418–2426. https://doi.org/10.1109/TNS.2013.2240697

Jamsen, T., Usoskin, I. G., Raiha, T., Sarkamo, J., & Kovaltsov, G. A. (2007). Case study of Forbush decreases: Energy dependence of the recovery. *Advances in Space Research*, *40*(3), 342–347. https://doi.org/10.1016/j.asr.2007.02.025

Kim, J., & Park, H. (2012). Development of a neutron energy monitoring system. *Progress in Nuclear Science and Technology*, *3*, 120–123. https://doi.org/10.15669/pnst.3.120

Kuzhevskij, B. M., Nechaev, O. Y., Panasyu, M. I., Sigaeva, E. A., Volodichev, N. N., & Zakharov, V. A. (2001). Neutron field of the Earth: Origin and dynamics. *Journal of Korean Association for Radiation Protection*, *26*(3), 315–319.

Lambert, D., Baggio, J., Hubert, G., Ferlet-Cavrois, V., & Flament, O. (2005). Neutron-induced SEU in SRAMs: Simulations with n-Si and n-O interactions. *IEEE Transactions on Nuclear Science*, *52*(6), 2332–2339. https://doi.org/10.1109/TNS.2005.860753

Lambert, D., Baggio, J., Hubert, G., Paillet, P., Girard, S., Ferlet-Cavrois, V., et al. (2006). Analysis of quasi-monoenergetic neutron and proton SEU cross sections for terrestrial applications. *IEEE Transactions on Nuclear Science*, *53*(4), 1890–1896. https://doi.org/10.1109/TNS.2006.880935

Leuthold, G., Mares, V., Rhüm, W., Weitzenegger, E., & Paretzke, H. G. (2007). Long-term measurements of cosmic ray neutrons by means of a Bonner spectrometer at mountain altitudes—First results. *Radiation Protection Dosimetry*, *126*(1–4), 206–511.

Libby, L. M., & Lukens, H. R. (1973). Production of radiocarbon in tree rings by lightning bolts. *Journal of Geophysical Research*, *78*, 5902–5903. https://doi.org/10.1029/JB078i026p05902

Lockwood, J. A., & Yingst, H. E. (1956). Correlation of meteorological parameters with cosmic ray intensities. *Physics Review*, *104*(6), 1718–1722. https://doi.org/10.1103/PhysRev.104.1718

Makhmutov, V.S., Bazilevskaya, G.A., Vashenyuk, E.V., Balabin, Yu.V., Gvozdevsky, B.B. (2008). Solar proton spectra in the 20 January 2005 GLE: Comparison of simulations with balloon and neutron monitor observations. *Physics of Auroral Phenomena, Proc. XXXI Annual Seminar*, Apatity, pp. 122-125.

Mangeard, P. S., Ruffolo, D., Sáiz, A., Madlee, S., & Nutaro, T. (2016). Monte Carlo simulation of the neutron monitor yield function. *Journal of Geophysical Research: Space Physics*, *121*, 7435. https://doi.org/10.1002/2016JA022638

Martin, I. M., & Alves, M. A. (2010). Observation of a possible neutron burst associated with a lightning discharge. *Journal of Geophysical Research*, *115*, A00E11. https://doi.org/10.1029/2009JA014498

Maurin, D., Cheminet, A., Derome, L., Hubert, G., & Melot, F. (2015). Neutron monitors and muon counters for solar modulation studies: Assessment of critical parameters in count rate calculations. *Advances in Space Research*, *60*(4), 833–847.

McCracken, K. G., Rao, U. R., & Shea, M. A. (1962). The trajectories of cosmic rays in a high degree simulation of the geomagnetic field. *M.I.T. Tech. Rep. 77, Lab. for Nucl.Sci. and Eng., Mass. Inst. of Technol., Cambridge*

Mironova, I. A., Usoskin, I. G., Kovaltsov, G. A., & Petelina, S. V. (2012). Possible effect of extreme solar energetic particle event of 20 January 2005 on polar stratospheric aerosols: Direct observational evidence. *Atmospheric Chemistry and Physics*, *12*(2), 769–778. https://doi.org/10.5194/acp-12-769-2012

Mishev, A., & Stamenov, J. (2009). Relation between rain flows and neutron flux at basic environmental observatory Moussala. *21st European Cosmic Ray Symposium*, Slovak Academy of Sciences, 132-135.

Mishev, A., Usoskin, I. G., & Kovaltsov, G. A. (2013). Neutron monitor yield function: New improved computations. *Journal of Geophysical Research: Space Physics*, *118*, 783–2788. https://doi.org/10.1002/jgra.50325

Mishev, A., Usoskin, I. G., Raukunen, O., Paassilta, M., Valtonen, E., Kovaltsov, G. A., & Vainio, R. (2018). First analysis of ground-level enhancement (GLE) 72 on 10 September 2017: Spectral and anisotropy characteristics. *Solar Physics*, *293*(136), 1–15.

Mishev, A. L., & Usoskin, I. G. (2016). Analysis of the ground-level enhancements on 14 July 2000 and 13 December 2006 using neutron monitor data. *Solar Physics*, *291*(4), 1225–1239. https://doi.org/10.1007/s11207-016-0877-2

Miyasaka, H., Takahashi, E., Shimoda, S., Yamada, Y., Kondo, I., Tsuchiya, H., et al. (2005). The solar event on 20 January 2005 observed with the Tibet YBJ neutron monitor observatory. *Proceedings of ICRC*, 241-244.

Moraal, H., Belov, A., & Clem, J. M. (1993). Design and coordination of multi-station international neutron monitor networks. *Space Science Reviews*, (1-2), 285–303.

Morishima, K., Kuno, M., Nishio, A., Kitagawa, A., Manabe, Y., Moto, M., et al. (2017). Discovery of a big void in Khufu's pyramid by observation of cosmic-ray muons. *Nature*, *552*(7685), 386–390. https://doi.org/10.1038/nature24647

Mrigakshi, A. (2012). Assessment of galactic cosmic ray models. *Journal of Geophysical Research*, 117, A08109. https://doi.org/10.1029/2012JA017611

Mrigakshi, A., Matthiä, D., Berger, T., Reitz, R., & Wimmer-Schweingruber, R. F. (2012). Assessment of galactic cosmic ray models. *Journal of Geophysical Research*, *117*, A08109. https://doi.org/10.1029/2012JA017611

Nagashima, K. (1990). Response and yield functions of neutron monitor, galactic cosmic-ray spectrum and its solar modulation derived from all the available world-wide surveys. *Proceedings of ICRC*.

Peronnard, P., Velazco, R., & Hubert, G. (2009). Real-life SEU experiments on 90 nm SRAMs in atmospheric environment: Measures vs. predictions done by means of MUSCA SEP3 platform. *IEEE Transactions on Nuclear Science*, *56*(6), 3450–3455.

Pioch, C., Mares, V., Vashenyuk, E. V., Balabin, Y., & Ruhm, W. (2011). Measurement of cosmic ray neutron with Bonner sphere spectrometer and neutron monitor at 79°N. *Nuclear Instruments and Methods in Physics Research A*, *626-627*, 51–57. https://doi.org/10.1016/j.nima.2010.10.030

Plainaki, C., Belov, A., Eroshenko, E., Mavromichalaki, H., & Yanke, V. (2007). Modeling ground level enhancements: Event of 20 January 2005. *Journal of Geophysical Research*, *112*, A04102. https://doi.org/10.1029/2006JA011926

Raukunen, O., Vainio, R., Tylka, A. J., Dietrich, W. F., Jiggens, P., Heynderickx, D., et al. (2018). Two solar proton fluence models based on ground level enhancement observations. *Journal of Space Weather and Space Climate*, *8*, A04. https://doi.org/10.1051/swsc/2017031

Reitz, G. (1993). Radiation environment in the stratosphere. *Radiation Protection Dosimetry*, *48*(1), 5–20.

Ricaud, P., Gabard, B., Derrien, S., Attié, J.-L., Rose, T., & Czekala, H. (2010). Valisation of tropospheric water vapor as measured by the 183-GHz HAMSTRAD radiometer over the Pyrenees mountains, Francea. *IEEE Transaction On Geoscience and Remote Sensing*, *48*(5), 2189–2203. https://doi.org/10.1109/TGRS.2009.2037920

Ricaud, P., Gabard, B., Derrien, S., Chaboureau, J.-P., Rose, T., Mombauer, A., & Czekala, H. (2010). HAMSTRAD-Tropo, a 183-GHz radiometer dedicated to sound tropospheric water vapor over Concordia station, Antarctica. *IEEE Transaction On Geoscience and Remote Sensing*, *48*(3), 1365–1380. https://doi.org/10.1109/TGRS.2009.2029345

Ricaud, P., Grigioni, P., Zbinden, R., Attié, J.-L., Genoni, L., Galeandro, A., et al. (2015). Review of tropospheric temperature, absolute humidity and integrated water vapour from the HAMSTRAD radiometer installed at dome C, Antarctica, 2009–14. *Antarctic Science*, *27*(06), 598–616. https://doi.org/10.1017/S0954102015000334

Rosolem, R., Shuttleworth, W. J., Zreda, M., Franz, T. E., Zeng, X., & Kurc, S. A. (2013). The effect of atmospheric water vapor on neutron count in the cosmic-ray soil moisture observing system. *Journal of Hydrometeorology*, *14*(5), 1659–1671. https://doi.org/10.1175/JHM-D-12-0120.1

Ruffalo, D., Saiz, A., Mangeard, P.-S., Kamyan, N., Muangha, P., Nutaro, T., et al. (2016). Monitoring short-term cosmic-ray spectral variations using neutron monitor time-delay measurements. *The Astrophysical Journal*, *817*(38), 1–12.

Rühm, W., Mares, V., Pioch, C., Simmer, G., & Weitzenegger, E. (2009). Continuous measurements of secondary neutrons from cosmic radiation at mountain altitude and close to the north pole—A discussion in terms of H*(10). *Radiation Protection Dosimetry*, *136*(4), 256–261. https://doi.org/10.1093/rpd/ncp161

Ryan, J. M., & Lee, M. A. (1991). On the transport and acceleration of solar flare particles in a coronal loop. *Astrophysical Journal*, *368*, 316. https://doi.org/10.1086/169695

Shea, M. A., Smart, D. F., & McCracken, K. G. (1965). A study of vertical cutoff rigidities using sixth degree simulations of the geomagnetic field. *Journal of Geophysical Research*, *70*, 4117–4130. https://doi.org/10.1029/JZ070i017p04117

Sidhu, S. K. (2017). A study of relation between sunspot numbers and occurrence of Forbush decreases. *International Journal of Pure and Applied Physics*, *13*(1), 244–247.

Usoskin, I. G., Alanko-Huotari, K., Kovaltsov, G. A., & Mursula, K. (2005). Heliospheric modulation of cosmic rays: Monthly reconstruction for 1951–2004. *Journal of Geophysical Research*, *110*, A12108. https://doi.org/10.1029/2005JA011250

Usoskin, I. G., Bazilevskaya, G. A., & Kovaltsov, G. A. (2011). Solar modulation parameter for cosmic rays since 1936 reconstructed from ground-based neutron monitors and ionization chambers. *Journal of Geophysical Research*, *116*, A02104. https://doi.org/10.1029/2010JA016105

Usoskin, I. G., Gil, A., Kovaltsov, G. A., Mishev, A., & Mikhailov, V. V. (2017). Heliospheric modulation of cosmic rays during the neutron monitor era: Calibration using PAMELA data for 2006–2010. *Journal of Geophysical Research: Space Physics*, *122*, 3875–3887. https://doi.org/10.1002/2016JA023819

Vos, E. E., & Potgieter, M. S. (2015). New modeling of galactic proton modulation during the minimum of solar cycle 23/24. *The Astrophysical Journal*, *815*(2), 119. https://doi.org/10.1088/0004-637X/815/2/119